**ORIGINAL PAPER**

# Synthesis, mechanical properties and enzymatic degradation of biodegradable poly(butylene carbonate-co-terephthalate)/ organically modified layered double hydroxide nanocomposites

Ming-Cheng Hsu[1] · Jie-Mao Wang[1] · Tzong-Ming Wu[1]

## Abstract
Two new various compositions of biodegradable aliphatic-aromatic poly(butylene carbonate-co-terephthalate) (PBCT) successfully synthesized through transesterification and polycondensation process were identified using $^1$H-NMR spectra. A series of PBCT/stearic acid-modified layered double hydroxide (SA-LDH) nanocomposites were fabricated using solution mixing process. The morphology of PBCT/SA-LDH nanocomposites were examined using wide-angle X-ray diffraction and transmission electron microscopy. Both results revealed that the stacking layers of SA-LDH were fully exfoliated into the PBCT polymer matrix. The storage modulus at −70 °C of PBCT/SA-LDH nanocomposites was greatly improved as compared to that of neat PBCT. The enzymatic degradation of PBCT/SA-LDH nanocomposites was examined using lipase from *Pseudomonas sp.* The weight loss of PBCT/SA-LDH nanocomposites increases with increasing loading of SA-LDH, recommending that the existence of SA-LDH enhances the degradation of the PBCT copolymers. This result might contribute to the lower degree of crystallinity for PBCT/SA-LDH nanocomposites. The result of MTT assay demonstrates that the PBCT/SA-LDH composites were appropriate for cell growth and might have a potential application used as biomedical materials.

**Keywords** Biodegradable · Aliphatic-aromatic copolyesters · Composites · Mechanical property · Enzymatic degradation

## Introduction

The synthetic polymers prepared using petrochemical products are extensively utilized in various arena because they are easy to fabricate and use. Additionally, their wastes were not cautiously handled after use due to their low costs and wide availabilities. Therefore, numerous investigations have aimed at biocompatible and biodegradable polymers for eco-friendly sustainability [1–6]. Biodegradable polymers, such as poly(butylene adipate) (PBA), poly(butylene succinate) (PBS), poly(butylene succinate-co-adipate) (PBSA), poly(butylene adipate-co-terephthalate) (PBAT), and poly(L-lactic acid) (PLLA), have been received considerable research attention from industrial and academic perspectives [7–12]. At present, commercial products of

PBS (Bionolle™, Showa Highpolymer), PBSA (BioPBS™, Mitsubishi), PBAT (Ecoflex®, BASF), and PLA (Ingeo™, NatureWorks) are immediately available on the market. Specially, the well-known aliphatic–aromatic PBAT synthesized via transesterification and polycondensation had presented their beneficial biodegradability of the aliphatic groups and excellent mechanical properties of the aromatic groups in their polymer backbones, which has been extensively used as agricultural films, compost bags, and packaging films [11].

Recently, aliphatic polycarbonates (APCs) have attracted most interests as biodegradable polymers, because of their biocompatibility, biodegradability, and nontoxicity [13, 14]. Compared with aliphatic polyesters, APCs can be synthesized using ring-opening polymerization method or copolymerization of $CO_2$ and epoxides [15, 16]. Among the producing APCs, poly(butylene carbonate) (PBC) has increased excessive interest due to its promising comprehensive properties and economical cost [17, 18]. However, a slow crystallization rate and a low melting temperature about 60 °C of PBC restricts its application variety and processing window. According to previous investigations, the incorporation of aromatic ester monomer into PBC backbone to form the

✉ Tzong-Ming Wu
  tmwu@dragon.nchu.edu.tw

1  Department of Materials Science and Engineering, National Chung Hsing University, 250 Kuo Kuang Road, Taichung 402, Taiwan

random poly(carbonate-co-ester)s could modulate the properties of PBC. This approach is similar to the preparation of PBA and PBAT. It was achieved that the crystallization property of PBA could be enhanced using copolymerizing with aromatic polyesters [19].

Therefore, this report focuses on synthesizing poly(butylene carbonate-co-terephthalate)s (PBCTs) copolymers with random conformations and desirable properties through transesterification and polycondensation procedure. Nonetheless, such a series of aliphatic–aromatic biodegradable copolymers based on PBC were rarely investigated [20, 21]. The new synthesized PBCT copolymers are expected to commercially available PBAT (Ecoflex®), which is a potential candidate for uses in polymer applications. In order to further enhance these mechanical and thermal physical properties, the incorporation of excellent physical properties of inorganic material served as the reinforcement into the PBCT copolymers can improve their physical properties [7, 22–24]. Reinforcing layered double hydroxides (LDH) has received numerous attentions owing to improve the physical properties of polymers [24–26]. The interlayered spacing of LDH is too small to fabricate the intercalated or exfoliated polymer nanocomposites. In order to enlarge the interlayered spacing of LDH, organo-modifiers with suitably functional group are necessary. Biocompatible stearic acid was selected in this study to manufacture the stearic acid-modified LDH (SA-LDH) via anion exchange method.

In this report, a series of poly(butylene carbonate-co-terephthalate)/stearic acid-modified layered double hydroxides nanocomposites were successfully synthesized. The microstructure, mechanical properties and enzymatic degradation of PBCT/SA-LDH nanocomposites were studied systematically. Finally, the capability of the PBCT/SA-LDH nanocomposites used as biomedical materials was examined via a 3-(4,5-dimethylthiazol-2-yl)-2,5-diphenyltetrazolium bromide (MTT) assay with L929 fibroblast cells.

## Experimental

### Materials

Stearic acid, potassium dihydrogen phosphate, and dipotassium hydrogenphosphate were purchased from J. T. Baker Chemical Company. Lipase from *Pseudomonas sp.*, 3-(4,5-dimethylthiazol-2-yl)-2,5-diphenyltetrazolium bromide (MTT), and dimethylsulfoxide (DMSO) were acquired from Sigma-Aldrich Chemical Company. Aluminum nitrate enneahydrate ($Al(NO_3)_3 \cdot 9H_2O$), 1,4-butanediol (BD), dimethylene carbonate (DMC), dimethylene terephthalate (DMT), and magnesium nitrate hexahydrate ($Mg(NO_3)_2 \cdot 6H_2O$) were obtained from Alfa Aesar Chemical Company. Sodium hydroxide was purchased from Fluka

Chemical Company. All chemicals were used without purification.

According to a previously published method, the synthesis of magnesium/aluminum layered double hydroxides (LDH) with molar ratio of Mg/Al = 2 were prepared via the coprecipitation from a mixing solution of 0.02 mol $Mg(NO_3)_2 \cdot 6H_2O$ and 0.01 mol $Al(NO_3)_3 \cdot 9H_2O$ in a 50 ml deionized water [25]. The mixing solution was stirred at room temperature under nitrogen gas to eliminate the formation of a carbonate. Then a 2M NaOH solution was added instantaneously to adjust at a fixed pH of 10, followed by constantly stirring at 90 °C for 24 h. The resulting product was filtered and washed with enormous volumes of deionized water to eliminate extreme salts. Finally, the fabricated LDH was dried in vacuum for 24 h. The synthesis of organically-modified LDH were prepared following the anion exchange method using LDH-NO3 as a precursor. A homogeneous aqueous solution containing an adequate amount of organo-modifier, stearic acid, was added to a suspension of LDH-NO3 in deionized water. The mixed aqueous solution was heated at 90 °C under a nitrogen gas protection for 24 h. The organically-modified LDHs were assigned as SA-LDH.

### Fabrication of PBCT/SA-LDH nanocomposites

The PBCT with molar ratios of [BC] to [BT] were 50:50 and 25:75, which were synthesized using transesterification and polycondensation; the resulting products are hereinafter designated as PBCT-50 and PBCT-25, respectively. In brief, suitable contents of BD, DMC, DMT and sodium hydroxide as a catalyst were mechanically stirred and heated at 120 °C for 1 h under nitrogen gas, and then heated to 190 °C for 1 h, and finally heated to 220 °C for 4 h in a vacuum of 67 Pa. For purification of PBCT copolymers, the as-synthesized PBCT was dissolved in 200 mL dichloromethane and then precipitated from 2 L cold methanol. The above purification process needs to repeat three times. Different amounts of PBCT-50, PBCT-25 and SA-LDH were individually dissolved in chloroform, and mixed/mechanically stirred for 3 days. The prepared PBCT-50/SA-LDH and PBCT-25/SA-LDH nanocomposites were washed and dried in vacuum.

### Methods

These measurements of small-angle X-ray scattering (SAXS) and wide-angle X-ray diffraction (WAXD) were performed using an X-ray diffractometer (Bruker D8) equipped with a Ni-filtered Cu Kα radiation source. In SAXS measurement, the q is the scattering vector defined as q = $(4\pi \sin\theta)/\lambda$, where λ is the X-ray wavelength. The sample to detector distance is about 300 mm. In WAXD measurement, the diffraction patterns were obtained in the range of 2θ = 1.5°–30° at a scanning rate of 1°/min. The

degree of crystallinity was determined using WAXD profile. The transmission electron microscopy (TEM) was carried out using Hitachi HF-2000. The specimens of TEM measurements encapsulated by epoxy were fabricated via a Reichert Ultracut ultramicrotome. Fourier transform infrared (FTIR) experiments were performed in the range of 400 to 4000 cm$^{-1}$ on a Perkin-Elmer Spectrum One spectrometer.

The crystalline melting temperature ($T_m$) for the PBCT and PBCT/SA-LDH nanocomposites was operated using a PerkinElmer Pyris Diamond DSC. All specimens were heated to the designed temperatures ($T_{ds}$) at a rate of 10 °C/min under nitrogen environment, which is about 30 °C higher than the $T_m$ of PBCT and held for 5 min to eliminate the residual crystals. Subsequently, they were cooled to $-50$ °C at a rate of 10 °C/min. Finally, the samples were heated to $T_{ds}$ at a rate of 10 °C/min and the $T_m$ for the PBCT and PBCT/SA-LDH nanocomposites are obtained.

$^1$H-nuclear magnetic resonance (NMR) spectra was measured using Agilet Technologies DD2 600 MHz NMR spectrometer via CDCl$_3$ as solvent and internal standard. The gel permeation chromatography (GPC) was used to confirm the weight-average molecular weight ($M_w$), number-average molecular weight ($M_n$), and polydispersity PDI $= M_w/M_n$ of the resulting polymers and composite materials. The narrow molecular-weight distributions of polystyrene standards were utilized as calibration. The storage modulus (E′) was carried out on a Perkin Elmer dynamic mechanical analyzer (DMA) from $-80$ to 140 °C at 2 °C/min heating rate and 1 Hz constant frequency.

The PBCT/SA-LDH nanocomposites were heat pressed at the temperature approximately 50 °C higher than its $T_m$ to fabricate the samples for enzymatic degradation analysis. All samples (10 mm × 10 mm) were put in 24-well plates containing 1 ml/mg lipase from *Pseudomonas sp.* The degraded samples were taken out at 3, 6, 9, and 12 days, washed with distilled water and vacuum dried. The amount of degradation was determined using the equation: $W_{weight\ loss}$ (%) $= 100[(W_0 - W_t)/W_0]$, where $W_0$ corresponds to the initial weight of a sample and $W_t$ is the weight of a sample after different degradation periods. The average values of at least three experiments are recorded.

L929 (BCRC RM60091, Hsinchu, Taiwan) cells were incubated on the tested samples for 12, 24, and 48 h. Cell suspensions were completely seeded over each of the samples in a 24-well plate. After the decided L929-cell incubation time, the cell growth was assayed through the MTT assay, in which tetrazolium salt is reduced to formazan crystals using the mitochondrial dehydrogenase of living cells. In brief, 3 h before the finish of the incubation time, 180 μL of Dulbecco's modified Eagle medium (DMEM; Gibco, Langley, OK) containing 1% penicillin/streptomycin and 20 μL of MTT solution were added to each well. Upon removal of the MTT solution, 200 μL of DMSO was also added to each well. The plates were then shaken until the formazan crystals had dissolved, and 150 μL of the solution from each well was transferred to a new 96-well plate. Plates were read using a BioTek Epoch spectrophotometer (Winooski, VT, USA) at 563 nm. Three independent measurements were used to determine the absorbance results.

## Results and discussion

### Synthesis, structure and morphology of various PBCT/SA-LDH nanocomposites

The compositions of PBCT-50 and PBCT-25 copolyesters were determined via $^1$H-NMR spectroscopy. Figure 1a and b show typical $^1$H-NMR spectra of the PBCT-50 and PBCT-25 copolymers in CDCl$_3$ with the assignment of each peak. As shown in this figure, the signals at $\delta = 7.24$ and 8.06 ppm correspond to CDCl$_3$ and the phenylene ($-C_6H_4-$) signal. Two signals at 4.19 and 4.13 ppm are assigned to hydrogen proton of $-CH_2O(CO)O-$ for the carbonate unit and the other signals at 4.41 and 4.36 ppm are assigned to hydrogen proton of $-CH_2O(CO)C_6H_4-$ for the ester unit [20, 21]. The chemical compositions of PBCT-50 and PBCT-25 copolymers estimated via the peak area ratio at $\delta = 4.41$–4.36 ppm to that at $\delta = 4.19$–4.13 ppm are recorded in Table 1. The ratios of carbonate unit to ester unit are approximately corresponding to the feed ratio of [BC] to [BT], recommending that the compositions of the fabricated PBCT-50 and PBCT-25 is consistent with that estimated around on the basis of the feed ratio. The weight average molecular weights and (Mw) and polydisperse index (PDI) of PBCT-50 copolymer determined using GPC are 44,980 g/mol and 1.73, respectively. The Mw and PDI of PBCT-25 is also listed in Table 1. The melting

**Table 1** Composition and molecular weight of synthesized polyesters

| Polymer | Feed Ratio [DMC]/[DMT] (mol %) | Polymer Ratio[a] [DMC]/[DMT] (mol %) | $M_w$ (g/mol) × 10⁴ | $M_n$ (g/mol) × 10⁴ | PDI | $T_m$ (°C) |
|---|---|---|---|---|---|---|
| PBCT-50 | 50/50 | 47.5:52.5 | 4.50 | 2.60 | 1.73 | 139.6 |
| PBCT-25 | 25/75 | 25.4:74.6 | 2.79 | 1.63 | 1.71 | 190.4 |

[a]Composition measured by $^1$H–NMR
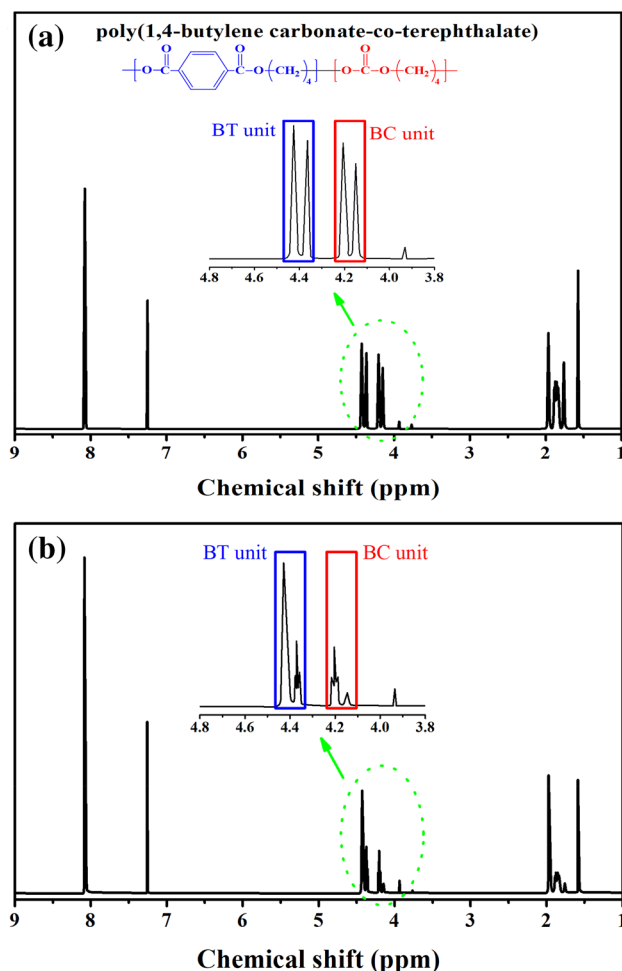
**Fig. 1** $^1$H–NMR spectra of the **a** PBCT-50 and **b** PBCT-25 copolyesters

temperatures of PBCT-50 and PBCT-25 determined by DSC are 139.6 and 190.4 °C, respectively.

The X-ray diffraction patterns of LDH and SA-LDH are presented in Fig. 2a. The data of LDH evidently reveal the formation of well stacked lamellae structure. The interlayer spacing of hydroxide layers was calculated to be 8.4 Å by means of the Bragg's equation. The XRD data of organically-modified LDH reveal that the main diffraction peak is shifted to lower angle with the incorporation of stearic acid, which indicates the interlayer spacing of hydroxide layers is expanded to 31.6 Å after the anionic exchange of stearic acid. The FTIR spectra of LDH and SA-LDH are shown in Fig. 2b. A broad absorption peak at about 3465 cm$^{-1}$ of all samples contributes to the stretching vibration of O–H group in the metal hydroxide sheets. Furthermore, two remarkable absorption peaks at 1385 cm$^{-1}$ and 1630 cm$^{-1}$ are obtained for the spectrum of LDH, which originate from the O–H bending of interlayer water molecules and antisymmetric stretching vibration of nitrate anions, respectively. After

the ionic exchange of nitrate using stearic acid, numerous typical absorption peaks are observed at 1415 cm$^{-1}$, 1550 cm$^{-1}$, 2855 cm$^{-1}$ and 2925 cm$^{-1}$. The corresponding absorption peaks at 1415 cm$^{-1}$ and 1550 cm$^{-1}$ are related to the symmetric and antisymmetric stretching vibrations of the COO– of carboxylate groups. The absorption peaks at 2855 cm$^{-1}$ and 2925 cm$^{-1}$ correspond to the C–H vibration mode of alkyl group. These data reveal that the functional group of stearic acid was up-taken by the sample. Both results of FTIR and XRD could suggest that the stearic acid has been efficiently exchanged and intercalated into the interlayers of LDH via the anionic exchange process. Therefore, a schematic representation of the probable arrangement for stearic acid-modified LDH is shown in Fig. 2c.

To evaluate the difference between LDH and stearic acid-intercalated LDH, the distortion and regularity of the crystalline lattice was analyzed by applying the Hosemann equation. The Hosemann equation is written as follows [25, 27]:

$$\delta^2 = \left(1/L_{hkl}^2\right) + (\pi gn)^4/d_{hkl}^2, \tag{1}$$

where δ is the half-width of diffraction peak, $L_{hkl}$ is the apparent correlation length perpendicular to the hkl crystal plane, g is the para-crystalline distortion parameter, n is the $n_{th}$ order diffraction peak, and $d_{hkl}$ is the interlayer distance. Figure 2d shows a plot of $\delta^2$ as a function of $n^4$ for LDH and SA-LDH. The values of g and $L_{hkl}$ were obtained from the slopes and intercepts of the curves. The $L_{hkl}$ values significantly increased from 78.2 Å for LDH to 154.0 Å for SA–LDH, and the g values decreased from 1.42–0.69%. These results showed that the correlation length increased and the para-crystalline distortion decreased for the organically modified LDH. According to the above results, we can assume that the structural arrangement of long-chain alkyl acid group-intercalated LDH had less defects for the layered hydroxides.

WAXD diffraction profiles of the PBCT-50/SA-LDH nanocomposites are presented in Fig. 3a. The diffraction peaks at 2θ = 16.2°, 17.3°, 20.6°, 23.4°, and 25.3° are obtained, which are corresponding to those of PBT crystallite [28, 29]. This finding demonstrates that the crystal structure of PBCT-50 is dominated by the crystalline PBT. For the samples of nanocomposites, they are also observed the same diffraction peaks as compared to that of PBCT-50. Nevertheless, no diffraction peak of SA-LDH obtained in the nanocomposite samples may be owing to the no regular periodicity of the stacked lamellar SA-LDH structure. The complete disappearance of the basal plane of SA-LDH leads to the formation of disordered and exfoliated arrangement within the PBCT matrix. Similar morphology and crystalline structure are also obtained for the PBCT-25/SA-LDH nanocomposites. Both crystalline structure of PBCT-50/SA-LDH and PBCT-25/SA-LDH nanocomposites are in the PBT
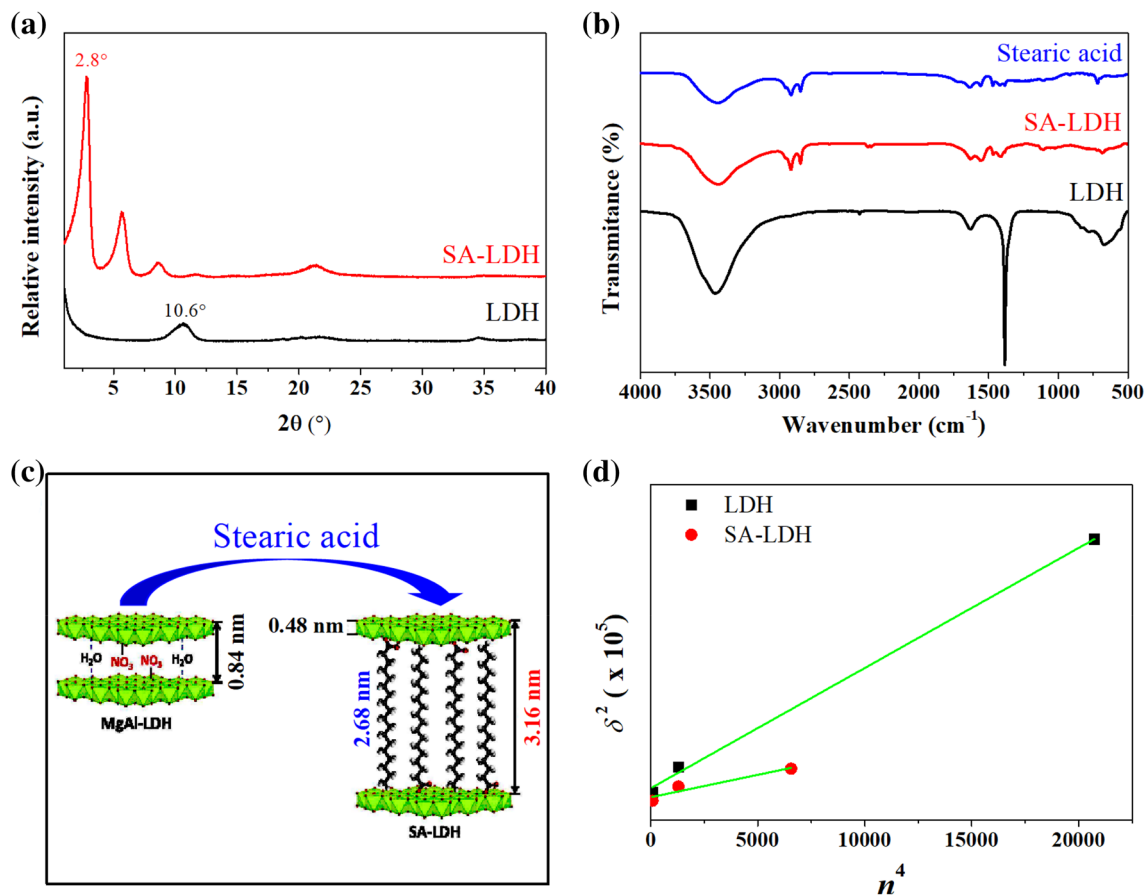
**Fig. 2** **a** X-ray diffraction patterns for LDH and SA-LDH. **b** FTIR spectra of LDH, SA-LDH and steric acid. **c** Schematic representation of the probable arrangement for stearic acid-modified LDH. and **d** Plots of $\delta^2$ versus $n^4$ for LDH and SA-LDH
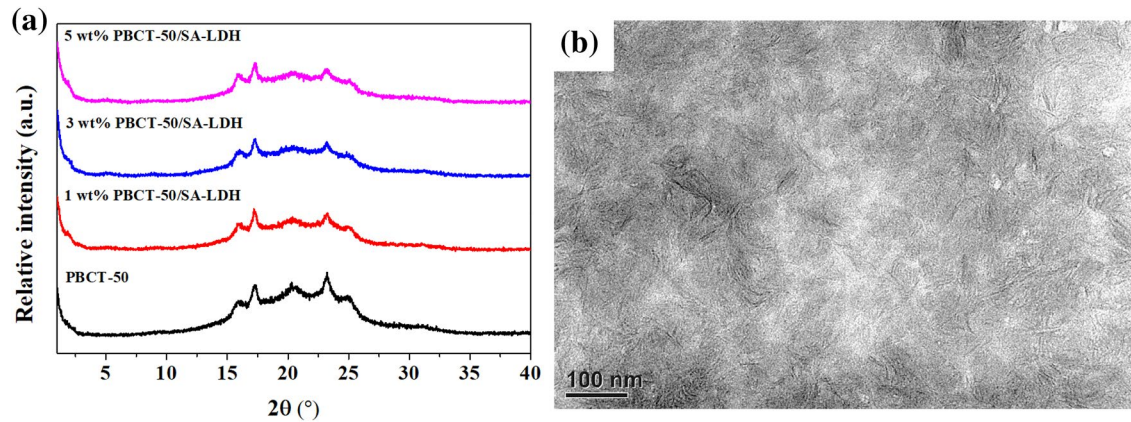


**Fig. 3** **a** WAXD patterns of PBCT-50 and various weight ratio of PBCT-50/SA-LDH nanocomposites. **b** TEM micrograph of 5 wt% PBCT-50/SA-LDH nanocomposites

crystalline form. Furthermore, the structural arrangement of 5 wt% PBCT/SA-LDH nanocomposites is wholly examined via TEM. Figure 3b presents TEM images of 5 wt% loading of SA-LDH into PBCT-50 copolymer matrices. This image shows that the stacking layer of the SA-LDH is randomly distributed into the PBCT-50 copolymers. Similar observation is also obtained for the PBCT-25/SA-LDH nanocomposites. Therefore, the exfoliated morphologies of PBCT/SA-LDH nanocomposites observed here using TEM are consistent with the diffraction data of WAXD.

The degree of crystallinity (*Xc*) of PBCT/SA-LDH nanocomposites evaluated using WAXD data is shown in Table 2. These results display the value of *Xc* of the PBCT-50/SA-LDH nanocomposites decrease with increasing the loadings of SA-LDH. This phenomenon contributes to the existence of SA-LDH in the PBCT-50 matrix, which can initiate more heterogeneous nucleation to produce more imperfect and tiny crystals, causing the decrease of *Xc*. Similar observations are also obtained for the PBCT-25/SA-LDH nanocomposites.

The microstructures of PBCT/SA-LDH nanocomposites were studied by SAXS. Figure 4a reveals the Lorentz-corrected SAXS profile of PBCT-50/SA-LDH nanocomposites. With the aim of examining the structural parameters in more detail, such as the lamellar thickness ($l_c$), long period ($L_p$), and the amorphous thickness ($l_a = L_p - l_c$), the one-dimensional correlation function was evaluated from Fourier transformation of Lorentz-corrected SAXS data by means of the equation as follows [30, 31]:

$$\gamma(z) = \frac{1}{Q} \int_0^\infty q I^2(q) \cos(qz) dq, \quad (2)$$

where $Q$ is the invariant, $z$ is the direction along which the electron density is measured, and *I(q)* is the Lorentz-corrected intensity.

The structural parameters of PBCT-50/SA-LDH nanocomposites are calculated from the typical profiles of one-dimensional correlation function presented in Fig. 4b. Similar results are also obtained for the PBCT-25/SA-LDH nanocomposites. The obtained structural parameters of PBCT/SA-LDH nanocomposites are presented in Table 2. For the PBCT-50/SA-LDH nanocomposites, $L_p$ was significantly higher than that of pure PBCT-50 polymer matrix and remained almost the same with the various SA-LDH contents. But the lc values gradually decrease as the SA-LDH contents increase. This result is possibly attributed to the incorporation of long-chain stearic acid, which might prevent the movement of PBCT-50 molecular chains to pack into the crystallites. Moreover, the la values slightly increase with increasing the content of SA-LDH. Consequently, *Xc* of the nanocomposites estimated via WAXD data was decreased with increasing the loading of SA-LDH. For the PBCT-25/SA-LDH nanocomposites, Lp was significantly lower than that of pure PBCT-25 polymer matrix and remained almost the same with the various SA-LDH contents. The tendency of lc and la values as well as the degree of crystallinity of PBCT-25/SA-LDH nanocomposites are similar to those of PBCT-25/SA-LDH nanocomposites.

## Physical properties of PBCT/m-LDH nanocomposites

Figure 5 presents the dependence of storage modulus *E′* versus temperature of PBCT-50/SA-LDH nanocomposites in a temperature ranging from −70 to 80 °C. The *E′* of PBCT-50 at −70 °C is around 347 MPa and decreases

**Table 2** Structural parameters, crystallinity, storage modulus at −70 °C and weight loss after 12 days degradation time of the various of PBCT and PBCT/SA-LDH nanocomposites

| Sample | $L_P$ (nm) | $l_c$ (nm) | $Xc$ (%) | $E'$ (MPa) | Weight loss (%) |
|---|---|---|---|---|---|
| PBCT-50 | 7.80 | 2.01 | 28.03 | 347 | 0 |
| 1 wt% PBCT-50/SA-LDH | 9.50 | 1.95 | 27.37 | 495 | 1.54 |
| 3 wt% PBCT-50/SA-LDH | 9.50 | 1.93 | 27.21 | 711 | 1.60 |
| 5 wt% PBCT-50/SA-LDH | 9.50 | 1.84 | 26.53 | 876 | 3.73 |
| PBCT-25 | 12.80 | 2.83 | 35.34 | 631 | 0 |
| 1 wt% PBCT-25/SA-LDH | 9.70 | 2.00 | 32.21 | 952 | 0.75 |
| 3 wt% PBCT-25/SA-LDH | 9.70 | 1.89 | 31.83 | 1288 | 0.77 |
| 5 wt% PBCT-25/SA-LDH | 9.70 | 1.75 | 30.67 | 1495 | 1.57 |

**Fig. 4** **a** Lorentz-corrected SAXS profiles and **b** one-dimensional correlation function calculated from the SAXS profiles for PBCT-50/SA-LDH nanocomposites
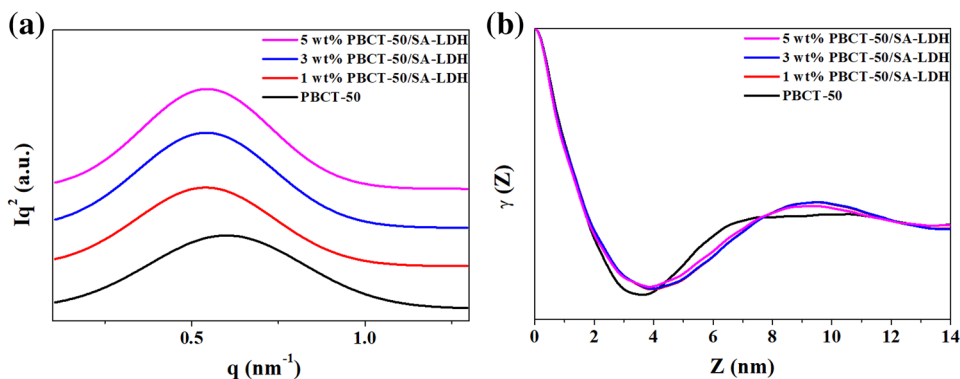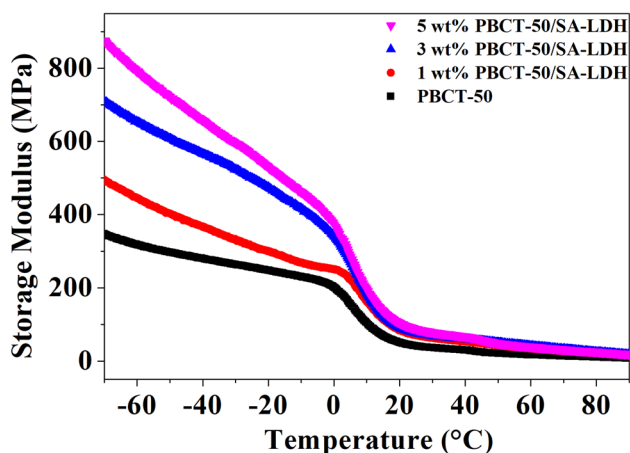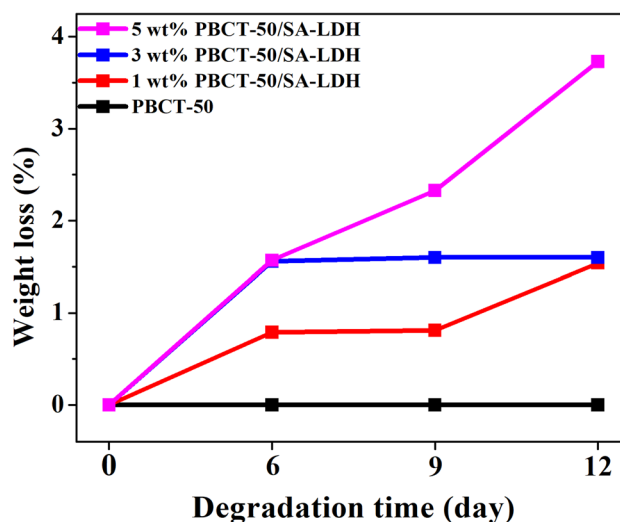
**Fig. 5** Dependence of the storage modulus on temperature of PBCT-50/SA-LDH nanocomposites



**Fig. 6** Dependence of the weight loss on the degradation time for the PBCT-50/SA-LDH nanocomposites

with increasing the temperature. This result suggests that the molecular motion of PBCT-50 is not enough in the glassy state, while the temperature larger than the glass transition temperature, the applied thermal energy ends up to be equivalent to the potential energy barriers of the molecular motions. The $E'$ of the PBCT-50/SA-LDH nanocomposites at −70 °C is increased with increasing loading of SA-LDH. Similar results are also obtained for the PBCT-25/SA-LDH nanocomposites. Detailed $E'$ for all PBCT/SA-LDH nanocomposites is also illustrated in Table 2. The $E'$ for the PBCT-25/SA-LDH nanocomposites are higher than those of PBCT-50/SA-LDH nanocomposites, which might be attributed to the presence of more rigid and aromatic BT groups. The improvement of $E'$ for the nanocomposites may contribute to the effect of adding inorganic and stiff stearic acid-modified LDH as a reinforcement, causing to the improvement on the rigidity of the PBCT polymer matrix.

For the enzymatic degradation test, the lipase from *Pseudomonas sp* was applied to examine the effect of SA-LDH on the enzymatic degradation behavior of the PBCT/SA-LDH nanocomposites. Since the crystalline structure of both PBCT system is in the PBT crystalline form and SA-LDH can't be degraded by lipase, the change of weight loss following enzymatic degradation is related with the chemical nature of PBCT copolymers. Figure 6 presents the weight losses of PBCT-50/SA-LDH nanocomposites through different degradation times. The weight loss of neat PBCT-50 after 12 days was almost unchanged; the weight losses for the PBCT-85/SA-LDH nanocomposites were 1.54%, 1.60%, and 3.73% with the loading of 1, 3, and 5 wt% SA-LDH, respectively. The weight loss tendencies of PBCT-25/SA-LDH nanocomposites were similar to those of the PBCT-50/SA-LDH nanocomposites. Detailed weight loss after 12 days degradation for all nanocomposites is also illustrated in Table 2. The weight loss of PBCT-50/SA-LDH

nanocomposites is slightly higher than those of PBCT-25/SA-LDH nanocomposites, which might be attributed to the presence of less rigid and aromatic BT groups. The weight loss increases with increasing the loading of SA-LDH, recommending that the existence of SA-LDH enhances the degradation of the PBCT copolymers. This result might contribute to the lower degree of crystallinity for PBCT/SA-LDH nanocomposites.

To observe the morphologies of all the samples after the degradation, we can utilize FESEM analysis. The FESEM images of the surfaces of all the samples before and after enzymatic degradation are shown in Fig. 7. Before enzymatic degradation, the surfaces of PBCT-50 were relatively smooth compared to those of all nanocomposites. After 3 days of degradation, the surface erosion with the presence of a small amount of porous and holes structures on PBCT/SA-LDH nanocomposites were observed. It can be seen that the roughness of the PBCT nanocomposites surface increase with an increase in the loading of SA-LDH, suggesting that the incorporation of the SA-LDH content into PBCT could enhance the degradation rate of PBCT.

Layered double hydroxides have demonstrated no significant cytotoxicity in the literatures [32–34]. New synthesized PBCT did not have any related reports about its cytotoxicity in the literatures. In this study, two series of biocompatible PBCT/SA-LDH composites were prepared using the solution mixing process. In the MTT assay, cell growth could be characterized using the optical density of purple formazan, which transformed from the MTT. The higher the absorbance, the larger amount of living cells [35]. After incubation times of 12, 24, and 48 h, the quantitative results of the MTT assay for the PBCT/SA-LDH nanocomposites are presented in Fig. 8. The obtained results revealed that the amount of
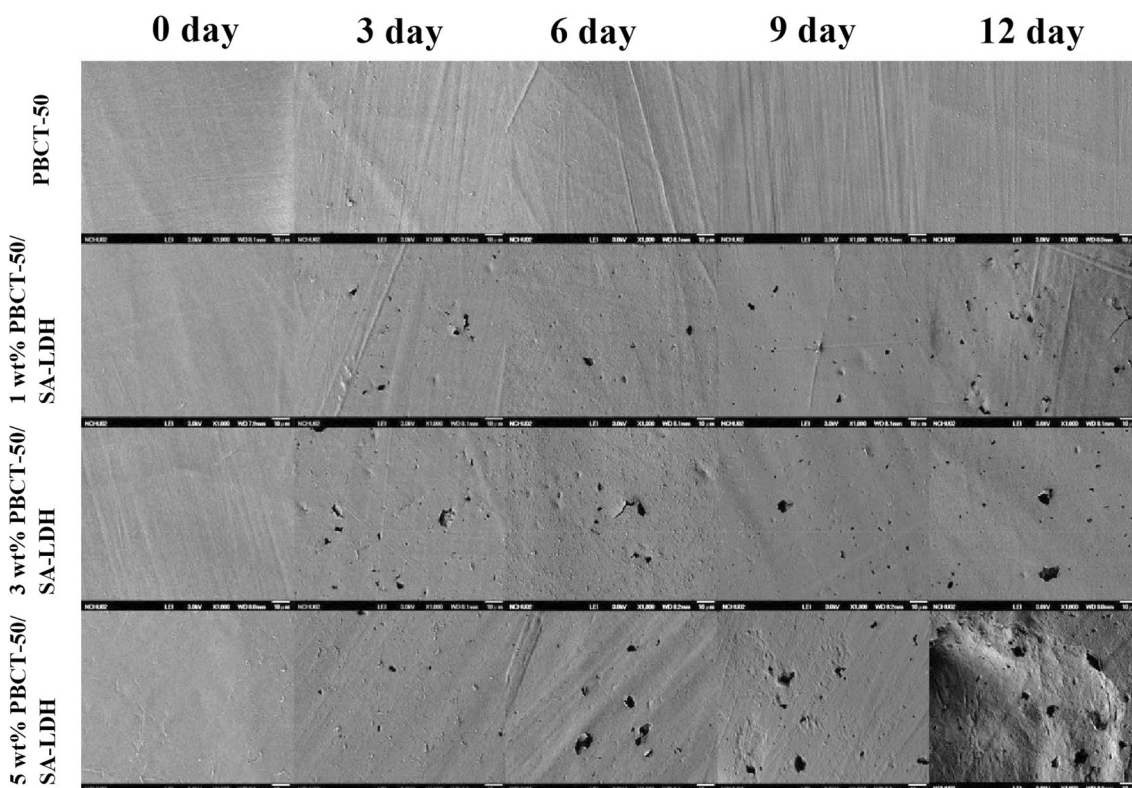
**Fig. 7** FESEM images of the enzymatically degraded PBCT-50/SA-LDH nanocomposites
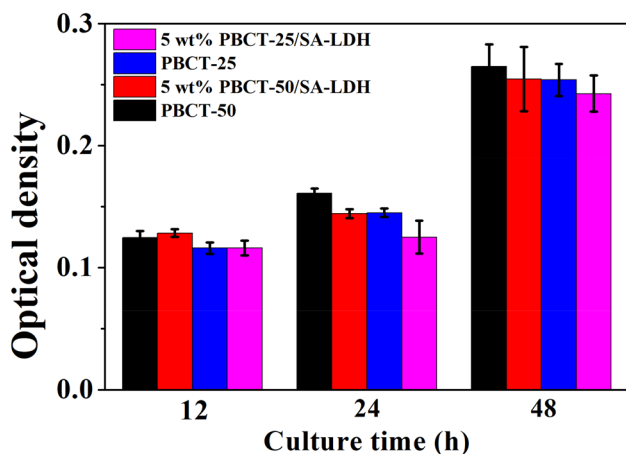


**Fig. 8** Biocompatibility of PBCT/SA-LDH seeded with L929 cells at various time points

the living L929 cell increased as the culture times increase in all samples. This observation suggested that the PBCT/SA-LDH nanocomposites synthesized in this work were appropriate for cell growth and might have a potential application as biomedical materials. This data also indicated that different contents of BT unit had a minor effect on cell growth. Nevertheless, the fabricated biodegradable nanocomposites might be considered as environmentally-friendly materials that can be usefully for the environmental sustainability.

## Conclusions

The new biocompatible and biodegradable PBCT/SA-LDH nanocomposites were manufactured using the transesterification and polycondensation process. Experimental results of WAXD and TEM indicated that the exfoliated conformations are formed for the PBCT/SA-LDH nanocomposites. The additional SA-LDH into PBCT matrix enhanced the storage modulus as compared to that of neat PBCT. The degradation rate of the neat PBCT-50 copolymer is silghtly higher than that of the PBCT-25 copolymer. The faster degradation rate of PBCT-50 is a result of the higher content of dimethylene carbonate unit and the chain flexibility of polymer backbone as compared to that of PBCT-25. Furthermore, the weight loss increases as the loading of SA-LDH increases, recommending that the existence of SA-LDH improves the degradation of the PBCT copolymers. This result might contribute to the lower degree of crystallinity for PBCT/SA-LDH nanocomposites. The results of the MTT assay indicated that the PBCT/SA-LDH composites may have a potential application for the biomedical material.

# References

1. Green DS, Boots B, Blockley DJ, Rocha C, Thompson R (2015) Impacts of discarded plastic bags on marine assemblages and ecosystem functioning. Environ Sci Technol 49(9):5380

2. Jambeck JR, Geyer R, Wilcox C, Siegler TR, Perryman M, Andrady A, Narayan R, Law KL (2015) Plastic waste inputs from land into the ocean. Science 347:768

3. Green DS, Boots B, O'Connor NE, Thompson R (2017) Microplastics affect the ecological functioning of an important biogenic habitat. Environ Sci Technol 51:68

4. Al-Sid-Cheikh M, Rowland SJ, Stevenson K, Rouleau C, Henry TB, Thompson RC (2018) Uptake, whole-body distribution, and depuration of nanoplastics by the scallop pecten maximus at environmentally realistic concentrations. Environ Sci Technol 52:14480

5. Kim JS, Lee HJ, Kim SK, Kim HJ (2018) Global pattern of microplastics (MPs) in commercial food-grade salts: sea salt as an indicator of seawater MP pollution. Environ Sci Technol 52:12819

6. Boots B, Russell CW, Green DS (2019) Effects of microplastics in soil ecosystems: above and below ground. Environ Sci Technol 53:11496

7. Chen YA, Chen EC, Wu TM (2015) Organically modified layered zinc phenylphosphonate reinforced stereocomplex-type poly(lactic acid) nanocomposites with highly enhanced mechanical properties and degradability. J Mater Sci 50:7770

8. Villegas C, Arrieta MP, Rojas A, Torres A, Faba S, Toledo MJ, Gutierrez MA, Zavalla E, Romero J, Galotto MJ, Valenzuela X (2019) PLA/organoclay bionanocomposites impregnated with thymol and cinnamaldehyde by supercritical impregnation for active and sustainable food packaging. Compos B: Eng 176:107336

9. Meng L, Yu L, Khalid S, Liu H, Zhang S, Duan Q, Chen L (2019) Preparation, microstructure and performance of poly(lactic acid)-poly(butylene succinate-co-butylene adipate)-starch hybrid composites. Compos B: Eng 177:107384

10. Kuo DL, Wu TM (2019) Crystallization behavior and morphology of hexadecylamine-modified layered zinc phenylphosphonate and poly(butylene succinate-co-adipate) composites with controllable biodegradation rates. J Polym Environ 27:10

11. Wang HT, Wang JM, Wu TM (2019) Synthesis and characterization of biodegradable aliphatic-aromatic nanocomposites fabricated using maleic acid-grafted poly(butylene adipate-co-terephthalate) and organically modified layered zinc phenylphosphonate. Polym Inter 68:1531

12. Wang X, Peng S, Chen H, Yu X, Zhao X (2019) Mechanical properties, rheological behaviors, and phase morphologies of high-toughness PLA/PBAT blends by in-situ reactive compatibilization. Compos B: Eng 173:107028

13. Feng J, Zhuo RX, Zhang XZ (2012) Construction of functional aliphatic polycarbonates for biomedical applications. Prog Polym Sci 37:211

14. Darensbourg DJ, Moncada AI (2010) Tuning the selectivity of the oxetane and $CO_2$ coupling process catalyzed by (Salen)CrCl/n-Bu$_4$NX: cyclic carbonate formation vs aliphatic polycarbonate production. Macromolecules 43:5996

15. Darensbourg DJ, Wilson SJ (2012) What's new with $CO_2$? Recent advance in its copolymerization with oxiranes. Green Chem 14:2665

16. Kricheldorf HR, Mahler A (1996) Polymers of carbonic acid 18: polymerizations of cyclobis(hexamethylene carbonate) by means of BuSnCl$_3$ or Sn(II)2-ethylhexanoate. Polymer 37:4383

17. Kricheldorf HR, Mahler A (1996) Polymers of carbonic acid. XVII. Polymerization of cyclobis(tetramethy1ene carbonate) by means of BuSnCl$_3$, and Sn(II)2-ethylhexanoate. J Polym Sci A Polym Chem 34:2399

18. Yamamoto Y, Kaihara S, Toshima K, Matsumura S (2009) High-molecular-weight polycarbonates synthesized by enzymatic ROP of a cyclic carbonate as a green process. Macromol Biosci 9:968

19. Wang HT, Chen EC, Wu TM (2020) Crystallization and enzymatic degradation of maleic acid-grafted poly(butylene adipate-co-terephthalate)/organically modified layered zinc phenylphosphonate nanocomposites. J Polym Environ 28:834

20. Zhang J, Zhu W, Li C, Zhang D, Xiao Y, Guan G, Zheng L (2015) Aliphatic–aromatic poly(butylene carbonate-co-terephthalate) random copolymers: synthesis, cocrystallization, and composition-dependent properties. J Appl Polym Sci. https://doi.org/10.1002/app.41952

21. Park GH, Lee S, Park SH, Eo SC, Kim JG, Lee BY (2016) Chopping high-molecular weight poly(1,4-butylene carbonate-co-aromatic ester)s for macropolyol synthesis. J Appl Polym Sci. https://doi.org/10.1002/app.43754

22. Wei Z, Lin J, Wang X, Huang L, Yu J, Li F (2015) In situ polymerization of biodegradable poly(butylene-co-succinate terephthlate) nanocomposites and their real-time tracking of microstructure. Compos Sci Technol 117:121

23. Salehabadi A, Bakar MA, Bakar NHH (2014) A. Effect of organomodified nanoclay on the thermal and bulk structural properties of poly(3-hydroxybutyrate)-epoxidized natural rubber blends: Formation of multi-components biobased nanohybrids. Materials 7:4508

24. Ciou CY, Li SY, Wu TM (2014) Morphology and degradation behavior of poly(3-hydroxybutyrate-co-3-hydroxyvalerate)/layered double hydroxides composites. Euro Polym J 59:136

25. Chiang MF, Chen EC, Wu TM (2012) Preparation, mechanical properties and thermal stability of poly(l-lactide)/γ-polyglutamate-modified layered double hydroxide nanocomposites. Polym Degrad Stab 97:995

26. Peng H, Han Y, Liu T, Tjiu WC, He C (2010) Morphology and thermal degradation behavior of highly exfoliated CoAl-layered double hydroxide/polycaprolactone nanocomposites prepared by simple solution intercalation. Thermochim Acta 502:1

27. Wu TM, Blackwell J, Chvalun SN (1995) Determination of the axial correlation lengths and paracrystalline distortion for aromatic copolyimides of random monomer sequence. Macromolecules 28:7349

28. Li F, Xu X, Hao Q, Li Q, Yu J, Cao A (2006) Effects of comonomer sequential structure on thermal and crystallization behaviors of biodegradable poly(butylene succinate-co-butylene terephthalate)s. J Polym Sci Polym Phys 44:1635

29. Zhang J, Wang X, Li F, Yu J (2012) Mechanical properties and crystal structure transition of biodegradable poly(butylene succinate-co-terephthalate) (PBST) fibers. Fibers Polym 13:1233

30. Strobl GR, Schneider M (1980) Direct evaluation of the electron density correlation function of partially crystalline polymers. J Polym Sci Polym Phys 18:1343

31. Barbi V, Funari SS, Gehrke R, Scharnagl N, Stribeck N (2003) SAXS and the gas transport in polyether-block-polyamide copolymer membranes. Macromolecules 36:749

32. Singh M, Singh RK, Singh SK, Mahto SK, Misra N (2018) In vitro biocompatibility analysis of functionalized poly(vinyl

chloride)/layered double hydroxide nanocomposites. RSC Adv 8:40611

33. Chiang MF, Wu TM (2010) Synthesis and characterization of biodegradable poly(L-lactide)/layered double hydroxide nano-composites. Compos Sci Technol 70:110

34. Chen YA, Tsai GS, Chen EC, Wu TM (2017) Thermal degradation behaviors and biodegradability of novel nanocomposites based on various poly[(butylene succinate)-co-adipate] and modified layered double hydroxides. J Taiwan Inst Chem Eng 77:263

35. Wei CK, Ding SJ (2017) Dual-functional bone implants with anti-bacterial ability and osteogenic activity. J Mater Chem B 5:1943